



STScI | SPACE TELESCOPE
SCIENCE INSTITUTE

When there is a discrepancy between the information in this technical report and information in JDox, assume JDox is correct.

JWST TECHNICAL REPORT

Title: NIRISS AMI Calibrator Requirements, Revision A.	Doc #: JWST-STScI-009180 Date: 15 January 2026 Rev: A
Authors: Phone: Deepashri Thatte, Kevin Volk, Rachel Cooper, Anand Sivaramakrishnan	Release Date: 4 February 2026

1 Abstract

The NIRISS Aperture Masking Interferometry (AMI) mode enables high-contrast, high-resolution imaging of sources around bright stars, and is designed to detect point sources that are separated by $\sim 75 - 500$ mas with a brightness ratio as small as 10^{-4} . The AMI mode requires a point spread function (PSF) reference star in addition to the science observation. The PSF reference star is used to calibrate out instrumental contributions to the interferometric observables of closure (or kernel) phases and visibility amplitudes that are used in determining detection limits of a faint companion near a bright source. The selection of the calibrator requires a match in spectral type and in brightness. We observed stars that are very similar in spectral type and brightness, stars of closely similar spectral types but somewhat different brightness, and stars of similar brightness but somewhat different spectral types as phase calibration standards to obtain more information about how sensitive the detection limits are to these factors. We find that matching brightness between target and calibrator is more important in improving contrast than matching spectral type.

2 Introduction

The Aperture Masking Interferometry (AMI) mode of JWST's NIRISS instrument uses a non-redundant aperture mask (NRM) in the pupil wheel with one of three medium-band filters (F380M, F430M, and F480M) and a wide-band filter (F277W) in the filter wheel. This mode provides the unique capability of high-contrast imaging at a separation of $\sim 75-500$ mas, which is not accessible to JWST's near-IR coronagraphs at similar wavelengths. The 7-hole mask turns the full aperture of the telescope into an interferometric array, that generates an interferogram in the image plane. AMI data reduction involves reducing these interferometric data to fringe

observables of closure phases (CP) and square visibility (SqV). The algorithm that is used to extract the observables from the image plane data is called the Lacour-Greenbaum algorithm (Lacour et al., 2011, Greenbaum et al. 2015) that is implemented in JWST AMI3 pipeline. In principle the closure phase is 0 for a perfect point source but in reality, there are systemic non-zero contributions to closure phases such as primary mirror imperfections and unequal path length errors. To remove this instrumental response a calibrator star is observed with the target and the closure phase of the calibrator is subtracted from the closure phase of the target. Similarly, the contribution of instrumental response to square visibility is removed by dividing the SqV of the target by SqV of the calibrator. The AMI noise sources and the effect on contrast have been discussed in detail in Greenbaum et al., 2015 and Sallum et al. 2024. The calibrator star is usually observed close to the target in time and sky position so that the JWST primary mirror configuration is the same during science and calibrator observations. The calibrated target observables are used to estimate binary point source contrast.

The goal of the analysis presented here is to determine how closely the phase calibration star needs to match the science target in brightness and spectral type. To do this we cross-calibrate the stars against each other and use the calibrated observables to estimate detection limits for combinations of spectral types and brightnesses.

3 Observations

CAL-NIRISS-214 (PID 4480)

Four stars with a range of spectral types and brightness were observed with NRM and F480M filter with SUB80 array at a single dither position POS1. The stars selected for the observations are HD 150668 (K0/1(III), WISE W2 = 4.937 ± 0.053), HD 149201 (K0III, WISE W2 = 4.973 ± 0.052), HD 149446 (K2III, WISE W2 = 5.393 ± 0.052) and IRAS 16516-1617 (M-giant, W2 = 5.408 ± 0.053). No spectral type is given for IRAS 16516-1617 in SIMBAD, but the Gaia prism spectrum shows that it is an M-type giant or supergiant.

Table 1 shows information about the observations from program 4480.

Table 1: Calibration program 4480 exposure information

Filename	Date/Time UTC	Target	Spectral Type	Brightness WISE W2	Pupil Filter	ngroups	nint	Total measured photons
jw04480001001_03102_00001_nis_calints.fits	2023-08-01 00:55:52.815	HD-150668	K0/1(III)	4.937 ± 0.053	NRM F480M	5	600	$6.56e8$
jw04480002001_03102_00001_nis_calints.fits	2023-07-31 23:38:13.492	HD-149201	K0III	4.973 ± 0.052	NRM F480M	5	600	$6.48e8$
jw04480003001_03102_00001_nis_calints.fits	2023-08-01 00:13:58.210	HD-149446	K2III	5.393 ± 0.052	NRM F480M	8	600	$6.99e8$
jw04480004001_03102_00001_nis_calints.fits	2023-08-01 01:37:46.045	IRAS-16516-1517	M-giant	5.408 ± 0.053	NRM F480M	8	600	$7.25e8$

The observations are designed such that the total number of photons in each exposure is about the same. According to [Ireland \(2013\)](#), the total number of photons is related to the contrast ratio by $1.5 \times N_{hole}^2 / (contrast\ ratio)^2$, where N_{hole} refers to the number of apertures (holes) in a mask. AMI NRM has 7 holes, therefore this translates to $73.5 / (contrast\ ratio)^2$. Since NRM is used for the first time in space we use a slightly more conservative value of $100 / (contrast\ ratio)^2$. The total number of measured photons in each exposure is $\sim 7e8$. The estimated contrast ratio (converted to magnitude) or the detection limit for all four stars is therefore 8.5 magnitudes. This achievable detection limit is therefore an expectation from photon noise.

4 Calibration and Analysis

The data were calibrated using JWST Detector 1, Image 2 and AMI3 pipeline (Bushouse et al. 2024) version 1.18.1. Program 4480 NRM and F480M data in SUB80 array were observed with NIRISS AMI template. The charge migration step was turned on at the Detector 1 stage; however it was not used because the PSF signal rates are below the charge migration threshold value. This threshold is the signal level at which charge migration causes the count rate of the peak pixel drop by 1%. When running the Image2 pipeline we skipped the photom step to leave the units of calibrated data in ADU/s instead of MJy/steradian. The resample step is also skipped for NIRISS AMI data. The AMI3 stage of the pipeline uses the steps `ami_analyze` and `ami_normalize`. In the `ami_analyze` step the `*_calints.fits` files for each star exposure were cropped so that the data is centered around the brightest pixel. Figure 1 shows a single integration of the cropped `calints.fits` file. `ami_analyze` step also fixes the bad pixels that are flagged as `DO_NOT_USE` in the DQ array by minimizing their Fourier power outside the region of support permitted by the pupil geometry. The method that is now part of the AMI3 pipeline was introduced by Ireland (2013) and implemented by Kammerer et al. (2019) as a standalone code.

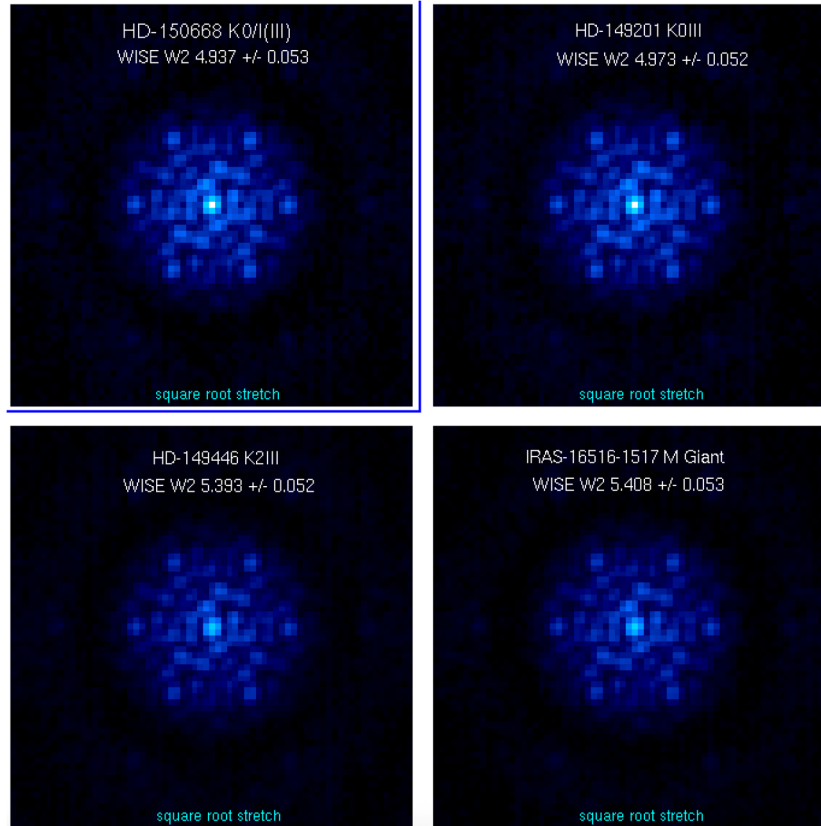


Figure 1: calibration program 4480 NRM + F480M data of 4 stars of same or different spectral types and brightness

The cropped calints.fits were analyzed to extract interferometric observables of closure phases and square visibilities. The resulting observables from `ami_analyze` are raw observables (Figure 2). that are calibrated with the observables of the calibrator star in the `ami_normalize` step.

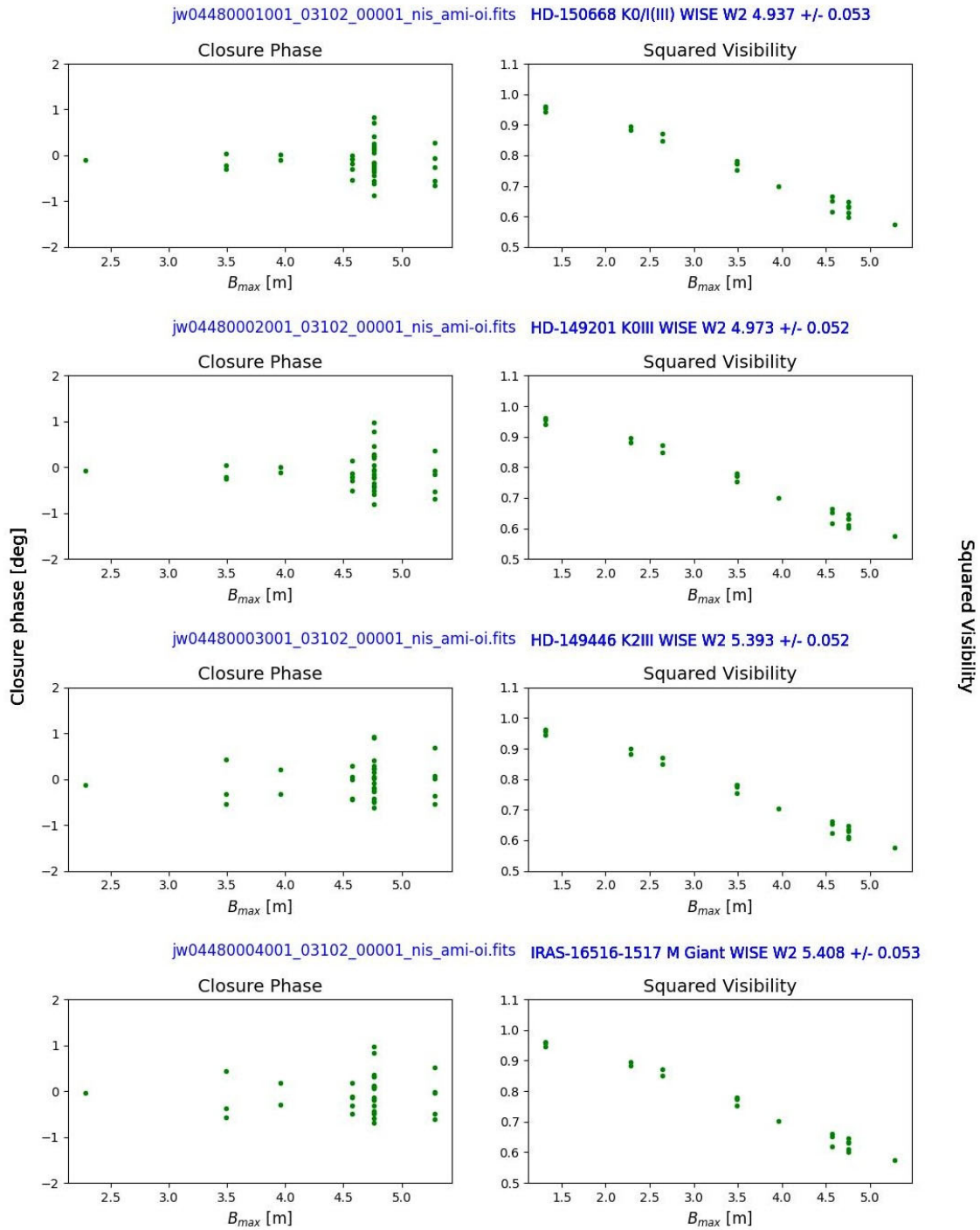


Figure 2: Raw interferometric observables of closure phases and square visibilities of the four stars.

The four stars were calibrated against each other to create 12 sets of calibrated observables for target-reference star pairs of star 1 calibrated by stars 2, 3 and 4, star 2 calibrated by stars 1, 3 and 4, star 3 calibrated by stars 1, 2 and 4, and star 4 calibrated by stars 1, 2 and 3. For each pair

the target's observables were normalized by those of the reference star, noting that star 1 calibrated by star 2 gives the same detection limits as star 2 calibrated by star 1. Figure 3 shows calibrated observables after dropping the duplicates.

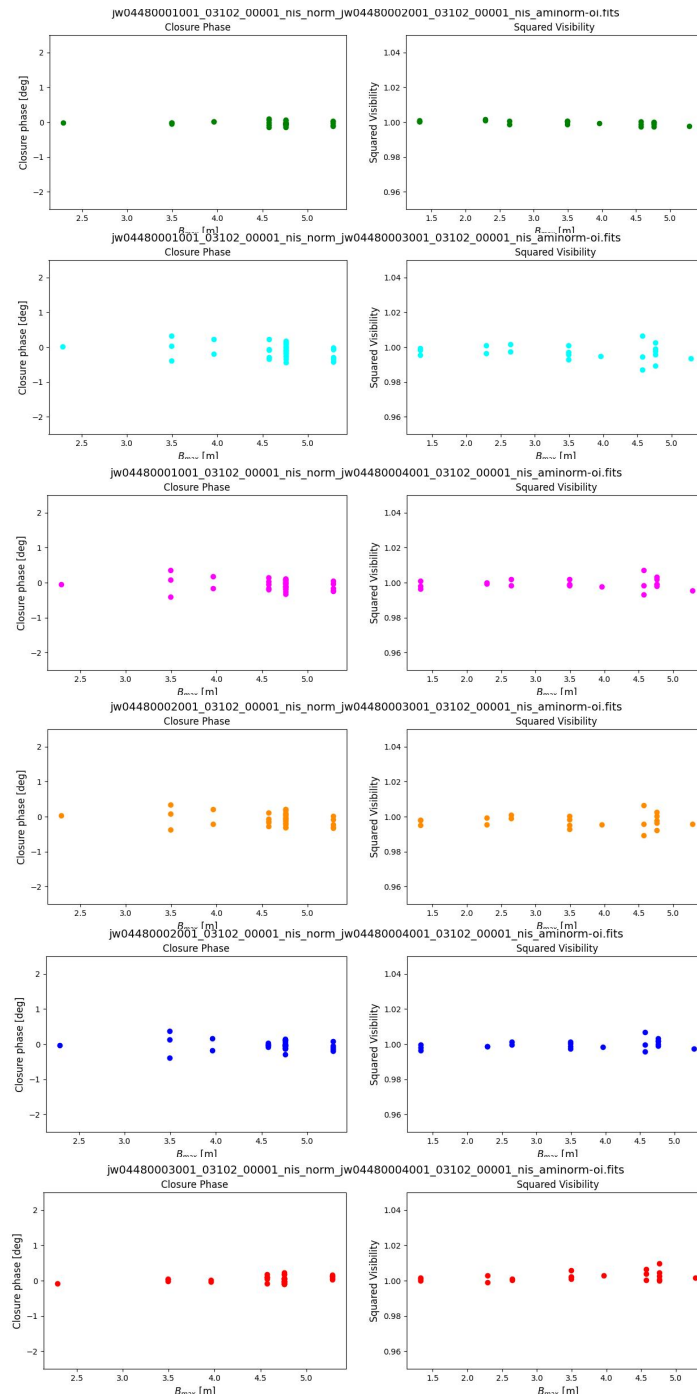


Figure 3. Calibrated closure phases and square visibilities of four stars calibrated against each other. Each target calibrator pair appears only once.

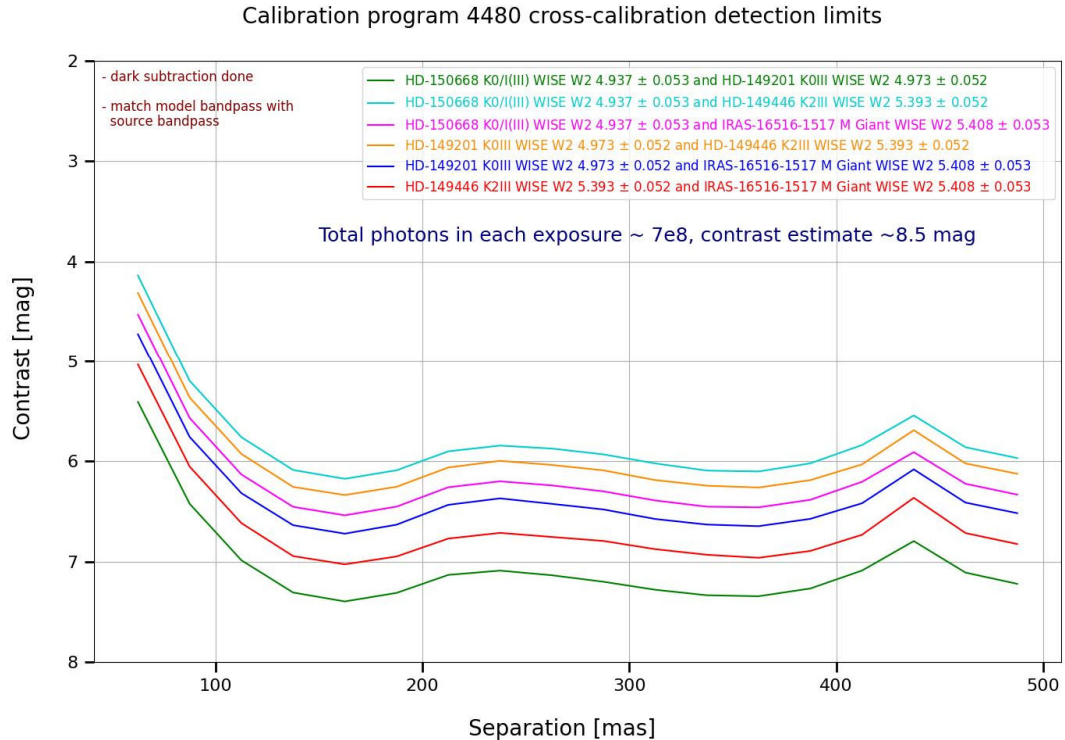


Figure 4: Detection limits from calibrated observables using Fourier

Detection limits were calculated using the toolkit Fourier described in Kemmerer et al. (2019), for each unique combination of two sources.

In this section and the next we use the same colors to identify target-calibrator pair calibrated observables, detection limits and highest contrast limits reached.

5 Results

The effect of spectral type and brightness match is shown in figure 4. We see the deepest contrast when the brightness and spectral type match closely as indicated by the green line. HD-150668, with spectral type K0/I(III), WISE W2 magnitude 4.937 ± 0.053 and HD-149201 with spectral type K0III and WISE W2 magnitude 4.973 ± 0.052 produce deepest contrast when calibrated with each other. These two sources are very close in brightness as well as spectral type as compared to other sources used as calibrators. The second deepest contrast curve is for the target-calibrator pair HD 149446, spectral type K2III, WISE W2 magnitude 5.393 ± 0.052 and IRAS 16516-1617 which is a M-giant with W2 magnitude of 5.408 ± 0.053 . These two sources are very close in brightness but not similar in spectral type. The difference in brightness for the four shallower curves is about 0.4 magnitudes while the difference in brightness for the deepest curves is 0.015 and 0.035 magnitudes respectively. The sources with brightness difference of 0.015 are also close in spectral type. Matching brightness seems to play a greater role in

achieving deeper contrast compared to spectral type. Figure 5 shows the plot of the Infrared Space Observatory short wavelength spectrograph spectra of late type stars in the spectral type range of the calibrator stars, from Sloan et al. (2003). The spectral shape overall is not too different between these different stars over the F480M filter passband, except for the differences in detail. This is also the reason that the spectral type matching is less important than the brightness matching, within this range of spectral types.

Comparison of Figure 3 and Figure 4 shows that the source pairs producing deepest contrast (green and red curves) have calibrated closure phases very close to zero and calibrated square visibilities very close to 1.

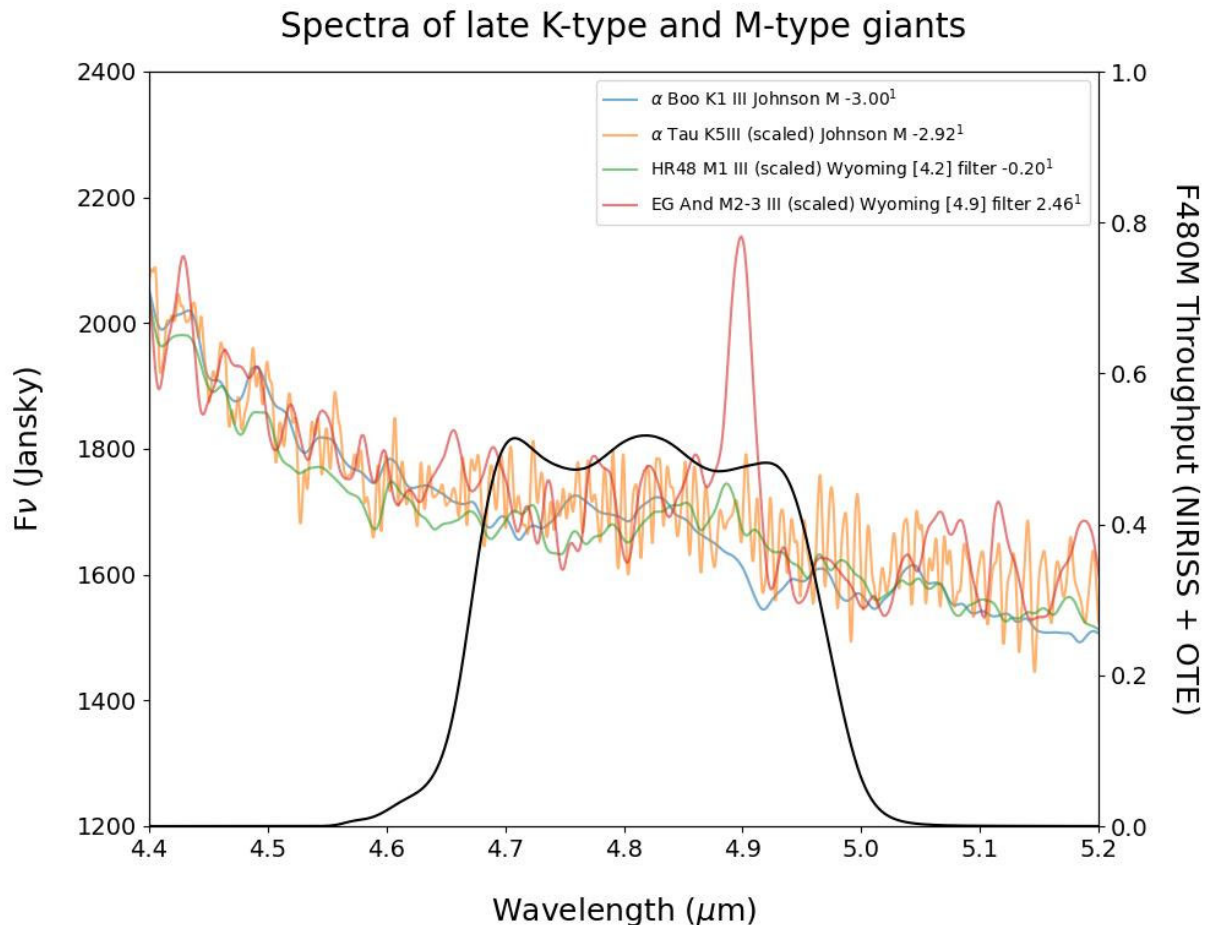


Figure 5. A plot of the Infrared Space Observatory short wavelength spectrograph spectra of late type stars in the spectral type range of the calibrator stars, from Sloan et al. (2003). The spectra have been scaled to match the level of alpha Boo in the F480M wavelength range. The response profile of the filter is overlaid for comparison. Over this spectral range there is not much variation of the overall spectral shape between types K1 III and M3 III, although there are variations in the molecular band features from star to star. Star EG And is somewhat fainter than the other stars whose spectra are shown and is correspondingly noisier, and therefore the peak at about 4.9 microns may be a noise spike on the spectrum.

¹: The stellar magnitudes in this figure represent the magnitudes of stars used to plot the spectra that are in the spectral type range of the calibrator stars. Please note that the magnitudes of these stars are not the same as magnitudes of calibrator stars that were observed.

6 Conclusion

We observed four stars with different spectral types and brightnesses with NIRISS NRM and F480M filter. The goal of the analysis is to determine how sensitive the detection limits are to mismatch between calibrator brightness and spectral type. Table 2 summarizes the information about the sources and the measured detection limits for target calibration pairs. $\sim 7 \times 10^8$ total photons were collected in each exposure, giving an achievable detection limit of 8.5 magnitudes.

Table 2: Contrast limits based on spectral type and brightness match

Target	Target calibrator pair						Highest Contrast reached mag
	Spectral Type	Brightness WISE W2	Total photons	Calibrator	Spectral Type	Brightness WISE W2	
HD-150668	K0/1(III)	4.937±0.053	6.58e8	HD-149201	K0III	4.973±0.052	~7.4
HD-150668	K0/1(III)	4.937±0.053	6.58e8	HD-149446	K2III	5.393±0.052	~6.2
HD-150668	K0/1(III)	4.937±0.053	6.58e8	IRAS-16516-1517	M-giant	5.408±0.053	~6.6
HD-149201	K0III	4.973±0.052	6.48e8	HD-149446	K2III	5.393±0.052	~6.3
HD-149201	K0III	4.973±0.052	6.48e8	IRAS-16516-1517	M-giant	5.408±0.053	~6.7
HD-149446	K2III	5.393±0.052	7.25e8	IRAS-16516-1517	M-giant	5.408±0.053	~7.00

We find that the target calibrator pair that has closest match in brightness and spectral type produces deepest contrast reaching ~ 7.3 magnitudes for the same number of total collected photons. Another target calibrator pair that has deep contrast of ~ 7 magnitudes has brightnesses that are very close but the spectral types are different. Comparison of two deepest detection limits shows that matching brightness between target and calibrator provides a better contrast than matching spectral type. Comparison of shallower detection limits with the deeper detection limits shows that brightness difference plays a significant role in reaching achievable contrast.

7 Acknowledgements

We are grateful to Steph Sallum for vetting the calibrators as single sources based for Keck AMI data, for doing spectral type mismatch simulations and analysis that were very helpful in

deciding the sources that were observed.

8 References

Bushouse, H., Eisenhamer, J., Dencheva, N., Davies, J., Greenfield, P., Morrison, J., Hodge, P., Simon, B., Grumm, D., Droettboom, M., Slavich, E., Sosey, M., Pauly, T., Miller, T., Jedrzejewski, R., Hack, W., Davis, D., Crawford, S., Law, D., Gordon, K., Regan, M., Cara, M., MacDonald, K., Bradley, L., Shanahan, C., Jamieson, W., Teodoro, M., Williams, T., & Pena-Guerrero, M. (2024). JWST Calibration Pipeline (Version 1.18.1) [Computer software]. <https://doi.org/10.5281/zenodo.7038885>

[Greenbaum A.Z., Pueyo L., Sivaramakrishnan A., Lacour S. 2015, *ApJ*, 798, 68](#)

An Image-Plane Algorithm for JWST's Non-Redundant Aperture Mask Data

[Ireland, M. J. 2013, *MNRAS*, 433, 2](#) Phase errors in diffraction-limited imaging: contrast limits for sparse aperture masking

Kammerer, J., Ireland, M. J., Martinache, F., & Girard, J. H. 2019, *MNRAS*, 486, 639: Kernel phase imaging with VLT/NACO: high-contrast detection of new candidate low-mass stellar companions at the diffraction limit. [DOI 10.1088/1538-3873/ac9a74](https://doi.org/10.1088/1538-3873/ac9a74)

Lacour, S., Tuthill, P., Amico, P., et al. 2011, *A&A*, 532, A72: Sparse aperture masking at the VLT. I. Faint companion detection limits for the two debris disk stars HD 92945 and HD 141569 <https://doi.org/10.1051/0004-6361/201116712>

Sallum S. *et al* 2024 *ApJL* **963** L2 The JWST Early Release Science Program for Direct Observations of Exoplanetary Systems. IV. NIRISS Aperture Masking Interferometry Performance and Lessons Learned, *ApJL* **963** L2 [DOI 10.3847/2041-8213/ad21fb](https://doi.org/10.3847/2041-8213/ad21fb)

Sloan et al. 2003, *ApJS*, 147, 379: A Uniform Database of 2.4-45.4 Micron Spectra from the Infrared Space Observatory Short Wavelength Spectrometer [DOI 10.1086/375443](https://doi.org/10.1086/375443)